Smoking Rain Clouds over the Amazon

M. O. Andreae,[1]* D. Rosenfeld,[2]* P. Artaxo,[3] A. A. Costa,[4] G. P. Frank,[1] K. M. Longo,[5] M. A. F. Silva-Dias[6]

Heavy smoke from forest fires in the Amazon was observed to reduce cloud droplet size and so delay the onset of precipitation from 1.5 kilometers above cloud base in pristine clouds to more than 5 kilometers in polluted clouds and more than 7 kilometers in pyro-clouds. Suppression of low-level rainout and aerosol washout allows transport of water and smoke to upper levels, where the clouds appear "smoking" as they detrain much of the pollution. Elevating the onset of precipitation allows invigoration of the updrafts, causing intense thunderstorms, large hail, and greater likelihood for overshooting cloud tops into the stratosphere. There, detrained pollutants and water vapor would have profound radiative impacts on the climate system. The invigorated storms release the latent heat higher in the atmosphere. This should substantially affect the regional and global circulation systems. Together, these processes affect the water cycle, the pollution burden of the atmosphere, and the dynamics of atmospheric circulation.

Several hundred thousand deforestation and agricultural fires burn in Amazonia during the dry season each year, covering vast areas with dense smoke (*1*, *2*). The smoke's radiative impact suppresses surface heating and evaporation and stabilizes the lower troposphere. In turn, this suppresses the formation of convective clouds and precipitation and thus slows down the hydrological cycle (*3*). The microphysical effects of the aerosols on clouds and precipitation are no less important but have until now only been inferred from modeling and satellite observations. Convective clouds forming in smoky air show substantially reduced droplet size compared to that of similar clouds in clean air (*4*), with a mean satellite-retrieved effective droplet radius of 9 μm in smoky clouds compared to 14 μm in clean clouds (*5*). This reduction of cloud droplet size by smoke is associated with an inhibition of the onset of precipitation radar echoes up to heights of ~6.5 km, compared to <3 km in smoke-free clouds (*6*, *7*).

Here, we report in situ measurements for validating the satellite inferences, comprising quantitative information on aerosols, cloud drop size distribution, and precipitation under a wide spectrum of conditions, from very clean air masses over the Equatorial Atlantic and the Amazon, through smoky air masses, to the extreme of pyro-clouds (i.e., clouds that form in the smoke plume over an active fire). Our results portray the following conceptual model of the various cloud and precipitation regimes:

(i) Blue ocean: Low concentrations of cloud condensation nuclei (CCN) in the clean atmosphere over the ocean produce clouds that are microphysically "maritime," i.e., have relatively few but large drops that coalesce rapidly into raindrops. In addition, the typically weaker updrafts over the ocean allow more time for raindrops to grow and precipitate before reaching the freezing level. Early precipitation further suppresses the updraft and vigor of the convection.

(ii) Green ocean: Over the unpolluted Amazon, especially in the rainy season, the aerosol concentration is almost as low as over the ocean (*8*). This is a result of effective aerosol washout by precipitation and of the feedback of the cleaned air to form clouds with even faster drop coalescence, precipitation, and aerosol washout. Therefore, clouds over the Amazon during the rainy season are predominantly microphysically maritime, hence the term "green ocean" (*9*).

(iii) Smoky clouds: Vegetation burning produces high concentrations of aerosols, a large fraction of which are capable of nucleating cloud droplets. This results in high concentrations of small cloud droplets that are slow to coalesce and precipitate. The lack of precipitation, except from the deepest clouds, keeps the particles in the air and creates a positive feedback for maintaining the smoky and rainless conditions. The lack of early precipitation allows updrafts to accelerate and transport cloud water in deep convection to the high and supercooled regions, where it can release additional latent heat of freezing, which it would not have delivered in the maritime case of early rainout. The added water is available for production of intense ice precipitation, hail, and lightning, creating more violent convective storms.

(iv) Pyro-clouds: These, the most extreme form of smoky clouds, feed directly on the smoke and heat from fires. They receive conflicting impacts: On one hand, extreme concentrations of CCN suppress the onset of precipitation, and the fire-generated heat invigorates the updrafts and further suppresses warm rain processes. On the other hand, large ash particles can serve as giant CCN and initiate large precipitation particles (*10*). This potential interaction of opposing effects is particularly pertinent in view of recent simulations (*11*) suggesting that there is a saturation to the suppression effects of aerosols with enhanced concentration, and that beyond a certain threshold very high concentrations result in recovery of drop size. However, the invigorated updrafts probably led to the observed enhancement of cloud drop concentrations in the pyro-clouds beyond that of the clouds growing from the smoky background.

Stronger atmospheric instability and a drier boundary layer can induce effects on clouds similar to those of the addition of aerosols, i.e., increasing updraft strength and cloud electrification (*9*). Separating the two effects represents a major challenge. To eliminate this factor as a major source of variability, we focus here on analyzing cases that had very similar thermodynamic structure of the atmosphere (Fig. 1 and fig. S1).

The SMOCC Campaign

The need to validate this conceptual model motivated the LBA-SMOCC (Large-Scale Biosphere-Atmosphere Experiment in Amazonia–Smoke, Aerosols, Clouds, Rainfall, and Climate) campaign from September to November 2002. At a ground site in Rondonia, Brazil, we made detailed measurements of the physical and chemical properties of the aerosol from the middle of the smoky dry season to the begin-

[1]Biogeochemistry Department, Max Planck Institute for Chemistry, Post Office Box 3060, D-55020 Mainz, Germany. [2]Institute of Earth Sciences, Hebrew University of Jerusalem, Jerusalem 91904, Israel. [3]Instituto de Fisica, Universidade de Sao Paulo, Rua do Matao, Travessa R, 187, CEP 05508-900, Sao Paulo, Brazil. [4]Universidade Estadual do Ceará, Avenida Paranjana, 1700, Campus do Itaperi, Fortaleza, CE, CEP 60740-000, Brazil. [5]Centro de Previsão de Tempo e Estudo Climáticos – Instituto Nacional de Pesquisas Espaciais (CPTEC-INPE), Rodovia Presidente Dutra, Km 40, SP-RJ, CEP 12630-000, Cachoeira Paulista, Sao Paulo, Brazil. [6]Departamento de Ciencias Atmosfericas, Instituto de Astronomia, Geofisica e Ciências Atmosfericas, Universidade de Sao Paulo, Rua do Matao, 1226 CEP 05508-900, Sao Paulo, Brazil.

*To whom correspondence should be addressed. E-mail: andreae@mpch-mainz.mpg.de (M.O.A., general issues); daniel.rosenfeld@huji.ac.il (D.R., cloud physics issues)

ning of the wet season, when pollution levels approach background conditions. We used two instrumented aircraft to characterize the range of aerosol and cloud ratios from pyro-clouds to pristine air (*12*). To investigate the role of smoke aerosols with minimal influence of changes in meteorological conditions, we conducted a set of flights on 4 and 5 October 2002, which went from a moderately polluted region in Rondonia to an area with very clean air over the western Amazon (Fig. 1). The air across the entire transect had originated from trade wind inflow across the northeastern coast of Brazil. Along the northern streamlines, this airmass remained without much contact with fires, whereas it received substantial regional pollution from fires in the southeastern part of our transect.

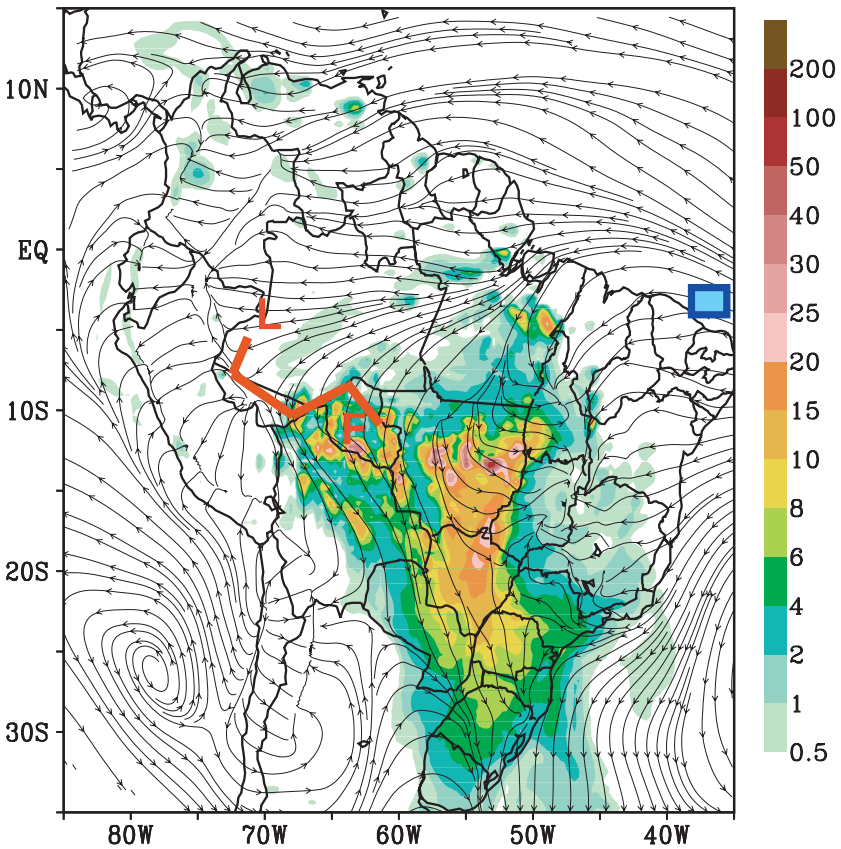

Fig. 1. Smoke aerosol distribution ($D < 2.5$ μm; in μg m^{-2}) and wind field in the BL over South America during the transect flights from Rondonia to the western Amazon. The aerosol distribution was obtained with the use of the Geostationary Operational Environmental Satellites–Automated Biomass Burning Algorithm (GOES ABBA) Fire product to estimate smoke emissions and the RAMS model to simulate their transport and removal (*38*). The flight track is indicated as a red line; the study area off Fortaleza, by a blue rectangle; and letters L and F represent the locations of the LET and FNS sounding sites, respectively (fig. S1).

Results

The fires emit smoke particles, which we quantified as condensation nuclei (CN) concentrations. The size distribution and composition of the CN determine the CCN spectrum, i.e., the CCN number concentration as a function of supersaturation. The CCN spectrum and the cloud base updraft velocity determine the cloud droplet size distribution (CDSD) at cloud base. The CDSD at cloud base controls most of the vertical evolution of CDSD in the growing convective elements, which in turn determines the height above cloud base (H) for onset of precipitation. The measured values for the four regimes (from blue ocean to the pyro-clouds) are summarized in Table 1.

Aerosols. Aerosol concentrations during LBA-SMOCC fell into three distinct ranges (Table 1): CN concentrations were near 500 cm^{-3} in the westernmost Amazon (Fig. 2) and at our ground site at the beginning of the rainy season. These values are slightly higher than the lowest campaign-average values observed previously over the Amazon [380 to 390 cm^{-3} (*8*, *13*)] and about twice as high as typical values in the marine boundary layer (MBL) over the Atlantic off Brazil. The slight enhancement observed during our campaign as compared to previous observations over Amazonia may be because of reduced washout during the dry season (previous data were from the wet season) or from minor smoke inputs.

In the smoky boundary layer (BL), mean CN levels were 2000 to 8000 cm^{-3}, with smoke plumes and haze layers often exceeding this range. These concentrations usually decreased into the cloud detrainment layer (CDL) and free troposphere (FT), but plumes and layers detrained from clouds gave rise to

Table 1. Representative values of CO, CN, CCN (1%), and cloud droplet number concentrations in the different regimes sampled during LBA-SMOCC (except where indicated otherwise). Also shown are the drop diameter of modal liquid water content, the height above cloud base to the onset of precipitation, and the cloud base height. Absolute cloud drop concentrations are obviously too high, at least in the clean conditions, for still-unexplained reasons, but we reported here the instrumental values. On the other side, quality control data of the SPP-100 show a severe undercounting because of coincidence of droplets in the measurement volume in the high aerosol situations. We report here the nominal values before attempting any corrections. D_L, drop diameter of modal liquid water content, is close to the effective radius but is not affected by truncation of the large drops because of instrument limitations. In situ onset of precipitation was defined as aircraft-radar rain echo and visible drops on the windshield. It occurred when LWC modal droplet diameter exceeded 24 μm. Numbers in brackets pertain to results from experiments in Thailand. Satellite onset of precipitation is on the basis of the 14-μm threshold for effective radius, from same day and area of the clouds sampled by the aircraft. Dash entries indicate data not available.

	CO (ppb)	CN (cm^{-3})	CCN at 1% SS (cm^{-3})	Cloud droplets (cm^{-3})	D_L (μm) at H = 1500 m	In situ H (m)	Satellite H (m)	Cloud base height (m)
Blue ocean	120*	100–350†	320	600	>30	1000	1100	400
Green ocean	140	500	340‡	1000	23–26	1500 [1400]	1500	1500 [1500]
Smoky Cb	200–650	2000–8000	1000–4000	2200	15–17	– [5200]	6700	1700 [2800]
Pyro-Cb	$1 \times 10^4 - 2.2 \times 10^4$§	$20 \times 10^4 - 44 \times 10^4$‖	$10 \times 10^4 - 23 \times 10^4$¶	2400	12	–	7800	1700

*From the Model of Atmospheric Transport and Chemistry (MATCH) for the region off the Brazilian coast, at the time and place of the blue ocean flights. †Data collected in the MBL over the Atlantic off Natal, Brazil, September 1989. ‡Because of instrument malfunction, CCN measurements were not possible during this period. The value shown is from the measured CN (500 cm^{-3}) and the CCN (1%)/CN ratio of 0.68 for the green ocean obtained during the LBA-CLAIRE-98 experiment. §Maxima observed during smoke plume passes. ‖Scaled from CO measurements with the use of observed $\Delta CN/\Delta CO = 20$ cm^{-3} ppb^{-1}. ¶Scaled from CN with the use of observed CCN/CN = 0.52.

elevated CN concentrations up to the highest accessible altitude (4300 m) (Fig. 2). The highest particle concentrations were present inside plumes over active fires and in pyro-clouds (Table 1).

The particle-size spectra of fresh (age of minutes to hours) smoke in plumes and in the BL with recent smoke inputs show little difference, having number-modal diameters around 100 nm. Cloud-processed or aged (days) particles in the regional haze and the aerosols in the clean (green ocean) BL are larger, with modal diameters around 130 to 170 nm. This shift in size distributions is consistent with the CCN behavior of the aerosol. CCN efficiency spectra (the ratio CCN/CN as a function of supersaturation, SS; Fig. 3) taken in the freshly polluted boundary layer show that about 40 to 60% of CN are able to nucleate cloud droplets at 1% SS, whereas the larger particles in aged smoke and in the clean BL have a distinctly higher efficiency (60 to 80%). Roberts *et al*. (*14*, *15*) have shown that the CCN properties of both pyrogenic and biogenic aerosols can be explained on the basis of their size-dependent chemical composition, which is characterized by a mixture of soluble inorganic and partially soluble organic constituents.

Cloud drop size distributions. The cloud physics aircraft made vertical cross sections near the tops of growing convective elements that grew in isolation or as well-defined feeders to cumulonimbus (Cb) clouds. The measurements were limited to altitudes below the zero isotherm (~4.8 km above mean sea level) because of aircraft constraints. The measured CDSD for the four regimes are provided in Fig. 4, A to D. A common feature is the widening of the CDSD with H, which can be depicted as the dependence of the drop diameter of modal liquid water content (D_L) on H (Fig. 5). When D_L exceeded 24 μm, warm rain was formed in the updraft in sufficient quantity to form radar echoes on the aircraft radar and make visible drops on the windshield. Often, rainfall was observed this way before being recorded by the X and Y probes, probably because of their small sampling volume.

Cloud base D_L shows small values for all cases. However, the shape of the CDSD does differ. Over the blue ocean, a wide tail of large drops occurs already at cloud base (Fig. 4A), apparently because of the large sea salt aerosols (*16*) that are present in the trade wind BL in sufficient quantities to induce such an effect (*17*). The surface wind during that flight was ~8 m s^{-1}, just enough to produce white caps and sea spray. The tail is much smaller in the green ocean (Fig. 4B), forming probably on large biogenic aerosols (*13*). The tail is smallest in clouds growing on the regional haze (Fig. 4C) but shows up in the pyro-clouds (Fig. 4D), apparently on the large ash particles. These ash particles range in size from sub-millimeter to a few centimeters and can remain airborne for relatively long times (minutes to hours) because of their low density and convoluted shape (*18*, *19*). They contain substantial amounts of soluble material and have been observed under the microscope to deliquesce at humidities >90%. This suggests that they are able to nucleate cloud drops quite readily. It is worth noting that the large-droplet tail is much smaller and appears at greater H in the pyro-clouds compared to the oceanic clouds. Furthermore, a pyro-Cb must reach $H > 7$ km for precipitating (Table 1). This shows that the ash particles play a less important role as giant CCN in the smoky clouds than do sea salt particles that are entrained into polluted clouds (*16*).

Substantial differences appear higher in the clouds. D_L at $H = 1000$ m is 10, 13, 23, and 25 μm for the four regimes, from the pyro to the blue, respectively (Fig. 5). Precipitation developed at H equal to 1000 and 1500 m over the blue and green oceans, respectively. According to the CDSD (Fig. 4, A and B), the large-drop tail at cloud base appears to have played a role in creating the raindrops over the ocean but not over the almost similarly pristine land and definitely not over the smoky land (Fig. 4C), at least up to the aircraft operational height limitation of 4.5 km. Satellite retrievals of cloud top particle effective radius (*20*) suggested that the precipitation threshold of 14 μm was exceeded at –22°C and –28°C, which correspond to H of 6600 and 7600 m for the smoky and pyro-clouds, respectively (Fig. 5).

The D_L for onset of precipitation was ~24 μm for the green ocean, consistent with the value over the blue ocean. We could not reach altitudes sufficiently high to establish D_L for the onset of precipitation in the smoky clouds. Instead, we used cloud physics aircraft measurements that were done identically, except for reaching $H > 7$ km, by the same flight scientist (D. Rosenfeld) as in SMOCC with similar aircraft instrument package during the Thailand cloud-seeding experiment (*21*). On 2 May 1998, the air was smoky from agricultural fires during the pre-monsoon in northwestern Thailand. The H-D_L relation on this day coincides at lower levels with the smoky curve of 4 October 2002 in Brazil and extends it to $H = 6400$ m (Fig. 5). Cloud liquid water content was >2 g m^{-3} up to the aircraft ceiling at the –31°C isotherm. Ice hydrometeors in the form of

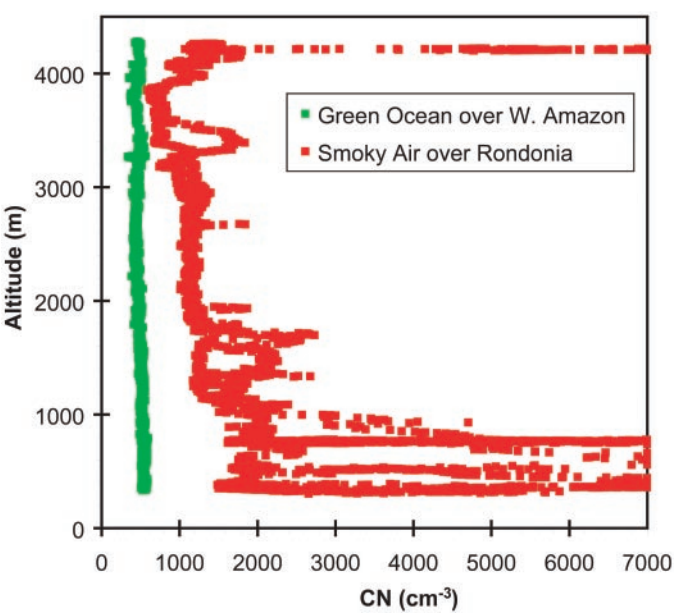

Fig. 2. Vertical distribution of CN over the smoky region in Rondonia and the clean region in the western Amazon sampled during the transect flights on 4 and 5 October 2002. The green ocean values are a composite of two soundings over the western Amazon and show little horizontal or vertical variability. The data from Rondonia also contain two soundings as well as data obtained during horizontal legs. They show a polluted BL below cloud base (at ~1000 m) and a somewhat less polluted CDL. Numerous plumes and haze layers are embedded in both the BL and the CDL. The layer at 4.2-km altitude had a minimal horizontal extent of about 12 km.

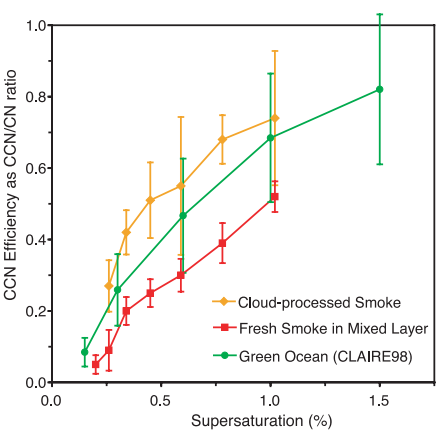

Fig. 3. Cloud droplet nucleating efficiency (expressed as the ratio of CCN to CN) as a function of supersaturation. Data are from flight SMOCC05 on 29 September 2002 for the smoky air and from CLAIRE-98 (*8*) for the green ocean.

frozen raindrops appeared at –22°C (H = 5200 m), where D_L reached 22 μm. Assuming a D_L = 24 μm threshold for warm rain, the cloud would have had to exceed H = 6400 m for producing warm rain under such smoky conditions. Obviously, any raindrop in such a low temperature would readily freeze and continue growing as hailstone or graupel. The preferential freezing of the larger drops probably curbed the rate of growth of D_L with H above the onset of ice precipitation at H = 5200 m.

In order to extrapolate the green ocean conditions to greater altitudes in a similar way, we used the Thai data from 16 July 1997, a typical continental monsoon day. The aircraft measurements showed the onset of warm rain at D_L = 24 μm. D_L kept growing up to 35 μm at H = 4200 m and –9°C, where these large drops started to freeze and left progressively smaller liquid droplets at greater heights and colder temperatures. Liquid cloud water decreased to less than 0.5 g m^{-3} at –16°C and was not detectable above the –27°C isotherm, even in the strongest updrafts (>20 m s^{-1}).

At the extreme end, pyro-clouds have the smallest D_L for the same H and reach only 16 μm at H = 3000 m, well below the size required for the onset of warm rain. According to analysis of MODIS (*22*) data (fig. S2), the onset of precipitation in these clouds occurs at the extremely large H of 7600 m.

Discussion

In spite of the different source mechanisms and compositions of the aerosol particles in smoky and clean regions and their vastly different concentrations, they are strikingly similar in their ability to nucleate cloud droplets. The aerosols over the green ocean are largely of biogenic origin (primary particles from the vegetation and gas-to-particle conversion from biogenic gaseous precursors). In contrast, the smoke is a mixture of ash particles, soot, organic materials, and inorganic salts (*23*–*26*). Both biogenic and pyrogenic particles consist predominantly of organic material [some 80% (*14*)], of which about 60% is water-soluble (*24*). Soluble inorganic salts (NH_4^+, K^+, SO_4^{2-}, and NO_3^-) represent most of the rest of the mass. Therefore, "conversion" of biological material to aerosol, whether through combustion or by "cold" processes, yields a material that is rather similar in its gross chemical composition and solubility in spite of considerable differences in the actual organic compounds present. This results in similar CCN properties for comparable size distributions and explains the similarity in CCN efficiency spectra between the green ocean and the cloud-processed smoke aerosols in the CDL (Fig. 3).

The smoke aerosols in the BL, with lower modal diameter, are somewhat "less efficient" CCN, i.e., have lower CCN/CN ratios. The age of these particles must be in the range of hours (given the abundance of fires in the region) to 1 to 2 days (the transit time across the region of burning). We observed only minor differences in size distribution between smoke sampled in the smoky BL and that in fresh plumes (age <30 min). Although we were not able to determine directly the CCN efficiency of smoke in fresh plumes, the similarity in size distribution suggests that it is similar to the smoky BL aerosol shown in Fig. 3.

Cloud properties are quite similar between the blue and green ocean regimes. With increasing aerosol concentrations, the clouds at first react very sensitively, through changes in the CDSD. When moving toward the pyro conditions, a given fractional addition in aerosol concentration is manifested as a smaller addition in cloud droplet concentration or a decrease in cloud drop size, but it does not completely saturate, in contrast to previous suggestions (*11*, *27*). This apparent contradiction may result from the fact that previous studies were concentrated in shallow clouds, whereas the current study is aimed at deeper, potentially precipitating clouds with stronger updrafts. Our findings show that the sensitivity to aerosols increases substantially with H (Fig. 5). This leads to profound differences in the precipitation processes, along the lines inferred by satellite observations (*6*, *7*, *20*).

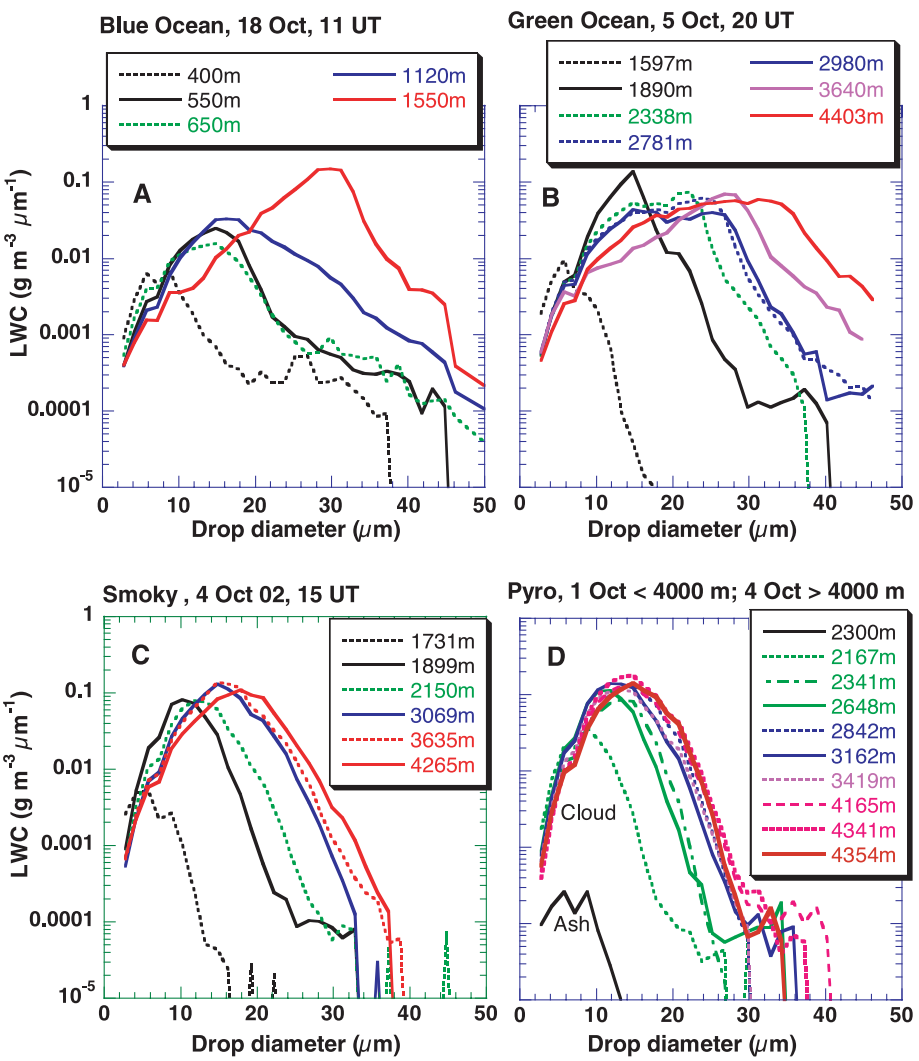

Fig. 4. The evolution of cloud drop diameter distribution (DSD) with height in growing convective clouds, in the four aerosol regimes of (**A**) blue ocean, 18 October 2002, 11:00 UT (universal time), off the northeast Brazilian coast (4S 38W); (**B**) green ocean, 5 October 2002 20:00 UT, in the clean air at the western tip of the Amazon (6S 73W); (**C**) smoky clouds in Rondonia, 4 October 2002, 15:00 UT (10S 62W); and (**D**) pyro-clouds, composite where clouds at height <4000 m are from 1 October, 19:00 UT (10S 56W), and clouds above 4000 m are from 4 October, 19:00 UT (10S 67W). The lowest DSD in each plot represents conditions at cloud base, except in (D), where a size distribution for large ash particles outside of the cloud is also shown. Note the narrowing of CDSD and the slowing of its rate of broadening with height for the progressively more aerosol-rich regimes from (A) to (D).

The shift of onset of precipitation to large H under smoky conditions leads to formation of large ice hydrometeors that were reported on the ground as large hail (up to 2 cm) and also produced small dents on the aircraft nose cone after flying in smoky conditions at cloud base level on 23 September 2002. This encounter occurred very near to the FNS sounding of 18 GMT (fig. S1), which did not show greater instability than the other soundings. It is remarkable that vigorous convection leading to intense thunderstorms and hail occurred in the smoky conditions (three cases were observed by the SMOCC team) in spite of the substantial reduction of surface solar heating by the smoke, with a seasonal average of –62.5 W m^{-2} (*28*). No reports of hail on the ground could be found for smoke-free conditions. Highly suppressed surface convective fluxes were also indicated by the smooth flying conditions experienced, even during midday in the smoky BL, to the extent of no discernible bumpiness. Cloud bases were poorly defined, and the clouds seemed to be merging in the vertical from ragged pieces at the lower levels. Clouds that rose above about 4 km became quite vigorous and, even when isolated, grew strongly and produced isolated intense showers and thunderstorms. Late in the day, these isolated clouds occasionally became organized into intense squall lines. Here, we see that, although the radiative effects of the smoke suppress the BL clouds, the microphysical effects overpower this radiative suppression and produce clouds that are more violent than can be found in microphysically maritime environments. These observations support suggestions (*9*, *29*) that aerosols play a major role in the determination of the dynamic, microphysical, and cloud electrification properties that distinguish continental from maritime convection (*30*).

Given that the suppression of initiation of precipitation is compensated by increased vigor of the storms, the net effect on the area amount of precipitation remains unknown. Owing to the decreased surface evaporation and the negative radiative forcing of –11.9 W m^{-2} at the top of the atmosphere (*28*), the overall hydrological cycle should be slowed down and regional precipitation should decrease under smoky conditions (*3*). However, feedbacks from the global circulation can change the local precipitation even more than the primary effect (*31*). In any case, the change from warm rain to ice precipitation should result in greater latent heat release higher in the clouds for the same rainfall amounts. This shift has the effect of enhancing planetary-scale upper-level waves that affect global climate (*32*, *33*).

An independent test of the importance of coagulation and precipitation in clouds can be made by examining the CN concentration (normalized to the conservative tracer, CO) in air detrained by clouds. Fresh plumes in SMOCC had a ΔCN/ΔCO ratio of 10 to 30 cm^{-3} parts per billion $(ppb)^{-1}$, comparable to values of 20 to 36 cm^{-3} ppb^{-1} reported from a savanna fire (*34*). Detrained haze layers in the CDL had ΔCN/ΔCO ratios in the same range, suggesting that little coagulation or scavenging had occurred. Even the highest layers encountered, such as the CN maximum at 4.2 km (Fig. 2), still showed ΔCN/ΔCO = 13 cm^{-3} ppb^{-1}. This indicates that, because of suppressed coalescence and precipitation, no more than a moderate amount of coagulation and scavenging could have occurred during convective transport, making it an efficient means to transport smoke aerosol at least to midtropospheric levels. Particle losses in deep tropical convection (*35*) might be greater (~75% of CN and 80 to 95% of accumulation mode particles), but, given the large amount of biomass smoke emitted in the tropics, even the 5 to 15% of the aerosol that survives transport to the upper troposphere is still a large contribution to this otherwise clean region.

The suppressed precipitation below $H = 6$ km can also explain the observation that smoky Cb in the tropics enrich the lower stratosphere with water vapor (*36*) by allowing a greater amount of cloud condensates in the form of smaller particles to detrain from cloud tops. Furthermore, this suppressed removal of water and smoke is coupled with invigoration of the updrafts and therefore greater likelihood for overshooting cloud tops into the stratosphere.

The positive feedback between aerosol concentration and reduced efficiency of precipitation scavenging may lead to a similar bistability of continental CCN levels and thermodynamic regimes over the Amazon, as has been proposed previously for the marine BL (*37*). In the green ocean regime, low CCN concentrations favor efficient precipitation scavenging, which in turn reduces CCN concentrations, until a balance between natural CCN production rates and precipitation removal is achieved. Interestingly, this balance occurs at CCN levels not very different from those over the blue ocean. In contrast, high CCN concentrations suppress wet removal, at least in the lower and middle troposphere, and thus stabilize the pollution burden. This favors the large-scale dispersal and upward transport as the dominant "sink" balancing regional pollutant emissions.

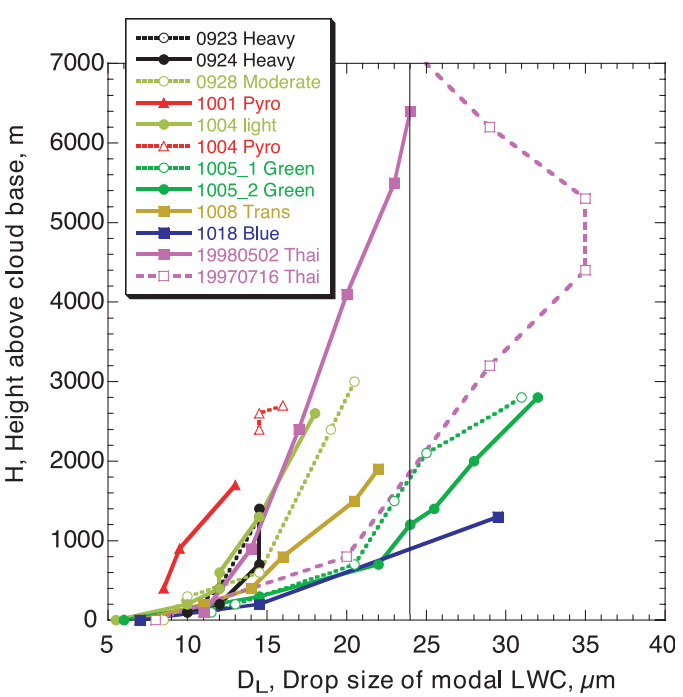

Fig. 5. The dependence of drop diameter of modal cloud liquid water content, D_L, on distance above cloud base, H, for the four aerosol regimes and transition situations. The vertical line at $D_L = 24$ μm denotes the onset of warm rain.

References and Notes

1. M. O. Andreae *et al.*, *J. Geophys. Res.* **107**, 10.1029/2001JD000524 (2002).
2. M. A. Silva Dias *et al.*, *J. Geophys. Res.* **107**, 10.1029/2001JD000335 (2002).
3. V. Ramanathan, P. J. Crutzen, J. T. Kiehl, D. Rosenfeld, *Science* **294**, 2119 (2001).
4. R. C. Eagan, P. V. Hobbs, L. F. Radke, *J. Appl. Meteorol.* **13**, 553 (1974).
5. Y. J. Kaufman, R. S. Fraser, *Science* **277**, 1636 (1997).
6. D. Rosenfeld, *Geophys. Res. Lett.* **26**, 3105 (1999).
7. D. Rosenfeld, W. L. Woodley, in *Cloud Systems, Hurricanes, and the Tropical Rainfall Measuring Mission (TRMM)*, W.-K. Tao, R. Adler, Eds. (American Meteorological Society, Boston, 2003), vol. 51, pp. 59–80.
8. G. C. Roberts, M. O. Andreae, J. Zhou, P. Artaxo, *Geophys. Res. Lett.* **28**, 2807 (2001).
9. E. Williams *et al.*, *J. Geophys. Res.* **107**, 10.1029/2001JD000380 (2002).
10. D. B. Johnson, *J. Atmos. Sci.* **39**, 448 (1982).
11. G. Feingold, L. A. Remer, J. Ramaprasad, Y. J. Kaufman, *J. Geophys. Res.* **106**, 22907 (2001).
12. Materials and methods are available as supporting material on *Science* Online.

13. P. Guyon *et al.*, *Atmos. Chem. Phys.* **3**, 951 (2003).
14. G. Roberts, P. Artaxo, J. Zhou, E. Swietlicki, M. O. Andreae, *J. Geophys. Res.* **107**, 10.1029/2001JD000583 (2002).
15. G. C. Roberts, A. Nenes, J. H. Seinfeld, M. O. Andreae, *J. Geophys. Res.* **108**, 10.1029/2001JD000985 (2003).
16. D. Rosenfeld, R. Lahav, A. Khain, M. Pinsky, *Science* **297**, 1667 (2002).
17. M. O. Andreae, S. J. de Mora, W. Elbert, *J. Geophys. Res.* **100**, 11335 (1995).
18. L. F. Radke *et al.*, in *Global Biomass Burning: Atmospheric, Climatic and Biospheric Implications*, J. S. Levine, Ed. (MIT Press, Cambridge, MA, 1991), pp. 209–224.
19. M. O. Andreae *et al.*, in preparation.
20. D. Rosenfeld, I. M. Lensky, *Bull. Am. Meteorol. Soc.* **79**, 2457 (1998).
21. D. Rosenfeld *et al.*, paper presented at the Seventh World Meteorological Organization Scientific Conference on Weather Modification, Chiang Mai, Thailand, 17 to 22 February 1999.
22. MODIS (Moderate Resolution Imaging Spectrometer) onboard NASA's AQUA satellite, passing over around 13:30 solar time.
23. B. Graham *et al.*, *J. Geophys. Res.* **107**, 10.1029/2001JD000336 (2002).
24. O. L. Mayol-Bracero *et al.*, *J. Geophys. Res.* **107**, 10.1029/2001JD000522 (2002).
25. R. J. Ferek, J. S. Reid, P. V. Hobbs, D. R. Blake, C. Liousse, *J. Geophys. Res.* **103**, 32107 (1998).
26. J. S. Reid *et al.*, *J. Geophys. Res.* **103**, 32,059 (1998).
27. J. S. Reid, P. V. Hobbs, A. L. Rangno, D. A. Hegg, *J. Geophys. Res.* **104**, 6145 (1999).
28. A. S. Procopio, L. A. Remer, P. Artaxo, Y. J. Kaufman, B. N. Holben, *Geophys. Res. Lett.* 2003GL018063RR (2003).
29. J. Molinié, C. A. Pontikis, *Geophys. Res. Lett.* **22**, 1085 (1995).
30. E. J. Zipser, *Mon. Weather Rev.* **122**, 1837 (1994).
31. F. J. Nober, H.-F. Graf, D. Rosenfeld, *Global Planet. Change* **37**, 57 (2003).
32. A. Kasahara, P. L. D. Dias, *J. Atmos. Sci.* **43**, 1893 (1986).
33. A. M. Grimm, P. L. D. Dias, *J. Atmos. Sci.* **52**, 3538 (1995).
34. P. V. Hobbs *et al.*, *J. Geophys. Res.* **108**, 10.1029/2002JD002352 (2003).
35. M. O. Andreae *et al.*, *Geophys. Res. Lett.* **28**, 951 (2001).
36. S. Sherwood, *Science* **295**, 1272 (2002).
37. M. B. Baker, R. J. Charlson, *Nature* **345**, 142 (1990).
38. S. R. Freitas, M. A. F. Silva Dias, P. L. Silva Dias, *Hybrid Methods Eng.* **2**, 317 (2000).

39. We thank all members of the LBA-SMOCC–Cooperative LBA Airborne Experiment 2002 and LBA–Radiation, Cloud, and Climate Interactions science teams for their support during the field campaign, especially J. von Jouanne, M. Welling, P. Guyon, G. Nishioka, T. Germano, and the pilots of the Universidad Estadual do Ceará (UECE) and Instituto Nacional do Pesquisas Espaciais (INPE) aircraft. We thank E. Freud for help with the scientific processing of the cloud physics aircraft data, M. Lawrence for providing results from the MATCH model, and E. Williams for stimulating discussions about the manuscript. This project was funded by the European Commission (Project SMOCC), the Max Planck Society, the Fundação de Amparo à Pesquisa do Estado de São Paulo, and the Conselho Nacional de Desenvolvimento Científico (Instituto do Milênio LBA).

Supporting Online Material

www.sciencemag.org/cgi/content/full/303/5662/1337/DC1
Materials and Methods
Figs. S1 to S10
References and Notes

11 December 2003; accepted 23 January 2004

REPORTS

Measurement of the Effect of Amazon Smoke on Inhibition of Cloud Formation

Ilan Koren,[1,2]* Yoram J. Kaufman,[1] Lorraine A. Remer,[1] Jose V. Martins[1,3]

Urban air pollution and smoke from fires have been modeled to reduce cloud formation by absorbing sunlight, thereby cooling the surface and heating the atmosphere. Satellite data over the Amazon region during the biomass burning season showed that scattered cumulus cloud cover was reduced from 38% in clean conditions to 0% for heavy smoke (optical depth of 1.3). This response to the smoke radiative effect reverses the regional smoke instantaneous forcing of climate from –28 watts per square meter in cloud-free conditions to +8 watts per square meter once the reduction of cloud cover is accounted for.

The net effect of aerosols on the atmospheric radiation budget and climate constitutes the greatest uncertainty in attempts to model and predict climate (*1*). Aerosols can counteract regional greenhouse warming by reflecting solar radiation to space or by enhancing cloud reflectance (*2*) or lifetime (*3*, *4*). However, aerosol absorption of sunlight is hypothesized to slow down the hydrological cycle and influence climate in ways not matched by the greenhouse effects (*5*, *6*). During periods of heavy aerosol concentration over the Indian Ocean (*7*) and Amazon basin (*8*), for example, measurements have revealed that absorbing aerosols warmed the lowest 2 to 4 km of the atmosphere while reducing by 15% the amount of sunlight reaching the surface.

Less irradiation of the surface means less evaporation from vegetation and water bodies, and (unless the smoke is concentrated near the surface only) a more stable and drier atmosphere, and consequently less cloud formation. This effect was defined theoretically as a positive feedback to aerosol absorption of sunlight (*9*) and was termed the semi-direct effect. A similar process, defined as cloud burning by soot, in which solar heating by the aerosol reaches its maximum near the top of the boundary layer, thereby stabilizing the boundary layer and suppressing convection, has been described (*10*). These cloud simulations were based on aerosol observations of INDOEX (Indian Ocean Experiment) (*11*) and focused mainly on the amplification of daytime clearing due to aerosol heating. Reduction of evaporation from the Mediterranean Sea by pollution from northern and eastern Europe was modeled to reduce cloud formation and precipitation over the Mediterranean region (*12*), in general agreement with measurements (*13*). However, warming of the atmosphere by similar widespread pollution aerosol over southeastern China was modeled to cause uplift of the polluted air mass over an area of 10 million km^2, which then was replaced by cooler moist air from the nearby Pacific Ocean, causing an increase in precipitation and flooding that fits observations from this region in recent years (*14*).

Here, using data from the MODIS-Aqua space instrument, we report measurements of the effect of smoke on cloud formation over the Amazon basin during the dry season (August–September) of 2002—namely, the reduction of the fraction of scattered cumulus clouds with the increase in smoke column concentration.

The area is under the influence of a regional high-pressure zone above a surface boundary layer and is associated with lower precipitation, land clearing, and biomass burning. The moisture source for the cloud formation and precipitation in the region is water vapor evaporated locally through plant evapotranspiration and moisture transported from the Atlantic Ocean (*15*), each responsible for half of the moisture that falls as precipitation. Easterly winds carry the moisture from the Atlantic Ocean throughout the Amazon basin until they reach the barrier of the Andes, where they decrease in velocity and veer either north or south (*16*) (Fig. 1).

The scattered cumulus clouds (also called boundary layer clouds) emerge regularly in the morning over the eastern shore. By local

[1]NASA Goddard Space Flight Center (GSFC), Greenbelt, MD 20771, USA. [2]National Research Council, Washington, DC 20001, USA. [3]Joint Center for Earth Systems Technology, University of Maryland, Baltimore County, Baltimore, MD 21250, USA.

*To whom correspondence should be addressed. E-mail: ilank@climate.gsfc.nasa.gov